Supporting Information

A new cholesterol-naphthalimide conjugate: Aggregation and sensing of CN⁻ and CO₂ under different conditions

Rameez Raza, Chiranjit Pati, Nabajyoti Baildya and Kumaresh Ghosh*

Department of Chemistry, University of Kalyani, Kalyani-741235, India.
Email: ghosh_k2003@yahoo.co.in; kumareshchem18@klyuniv.ac.in

Table S1. Results of gelation test for compound **1**.

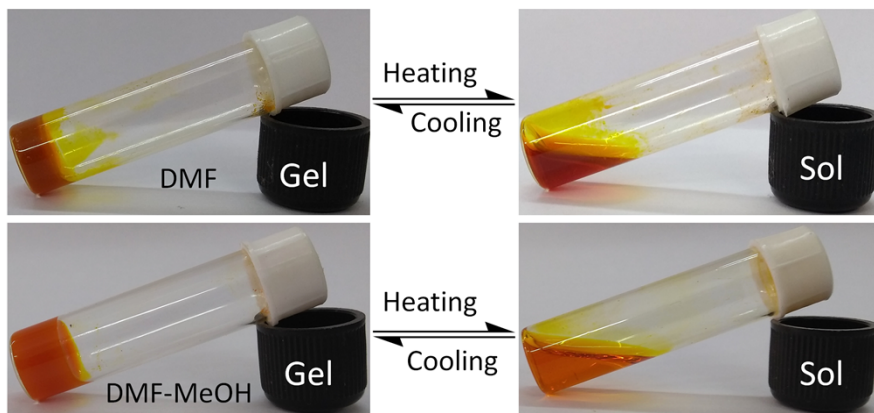| Solvent	1
DMSO	S
DMF	**G (50 mg/mL)**, (T_{gel}= 36 ^{O}C)
CH_3CN	PS
THF	S
$CHCl_3$	S
MeOH	I
Toluene	PS
Benzene	PS
$DMSO-H_2O$ (1:1, v/v)	P
$DMF-H_2O$ (1:1, v/v)	P
CH_3CN-H_2O (1:1, v/v)	P
DMF-MeOH (1:1, v/v)	**G (10 mg/mL)**, (T_{gel}= 54 ^{O}C)
1,4-Dioxane	PS
$1,4-Dioxane-H_2O$ (1:1, v/v)	P
Hexane	I
S = Solution; I = Insoluble; PS = Partially soluble; P = Precipitation, G= Gel	

Figure S1. Thermo-reversibility of gel **1** [c= 6.1 x 10^{-2} M (for DMF gel) and c= 1.2 x 10^{-2} M (for DMF-MeOH gel)].
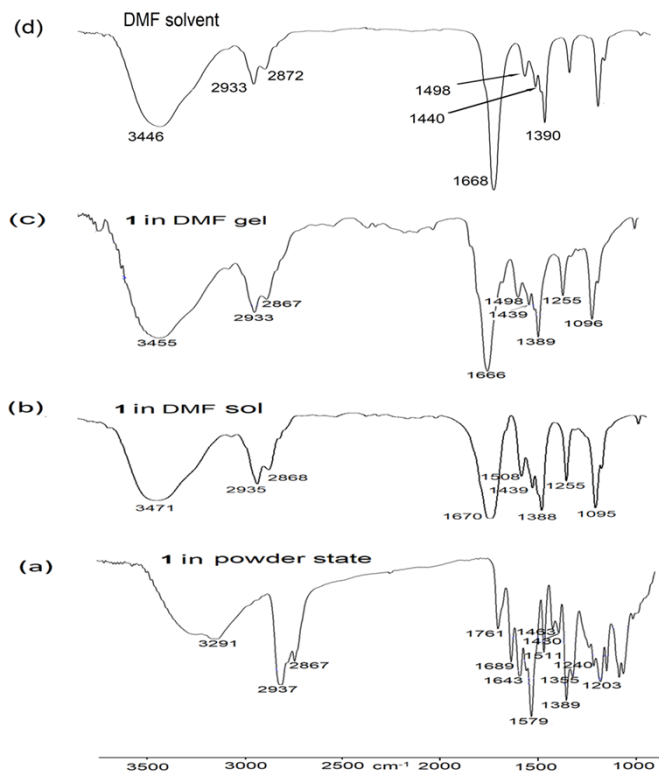

Figure S2. Comparison of FTIR spectra of **1** in the (a) powder, (b) solution and (c) gel state in DMF. In the series, (d) indicates the FTIR of DMF solvent.
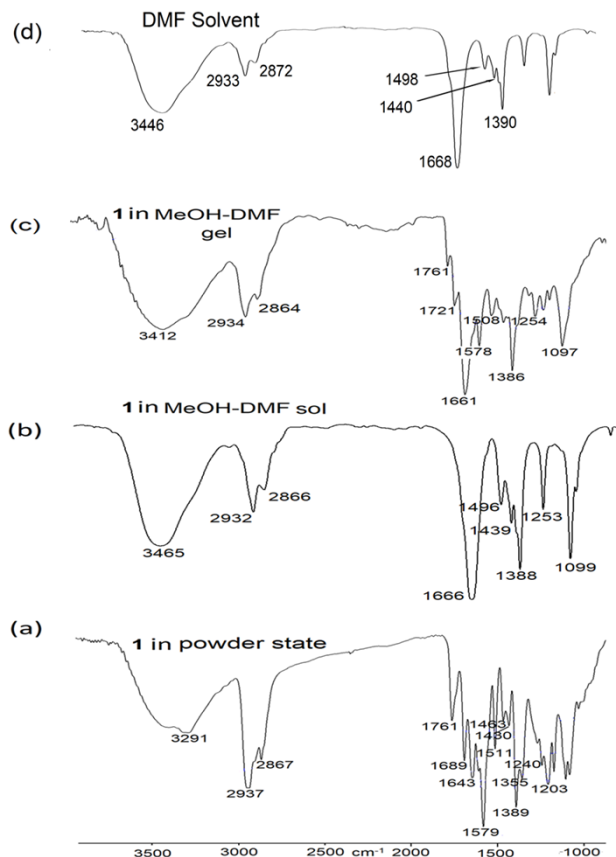
Figure S3. Comparison of FTIR spectra of **1** in (a) powder, (b) solution and (c) gel states in DMF-MeOH (1: 1, v/v). In the series, (d) indicates the FTIR of DMF solvent.
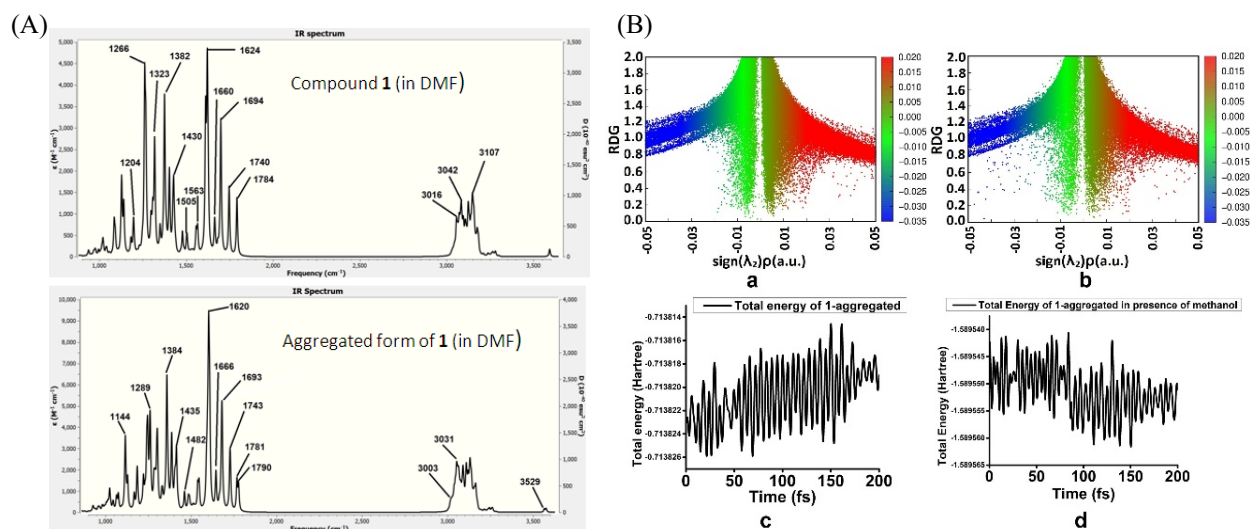

Figure S4: (A) Theoretical FTIR spectra of **1** and its aggregated form in DMF; (B) Reduced density gradient plots of **1**-aggregated form in (a) DMF, (b) DMF-CH$_3$OH; ADMP trajectories of optimized geometry of **1**-aggregated form in (c) DMF and in presence of CH$_3$OH.
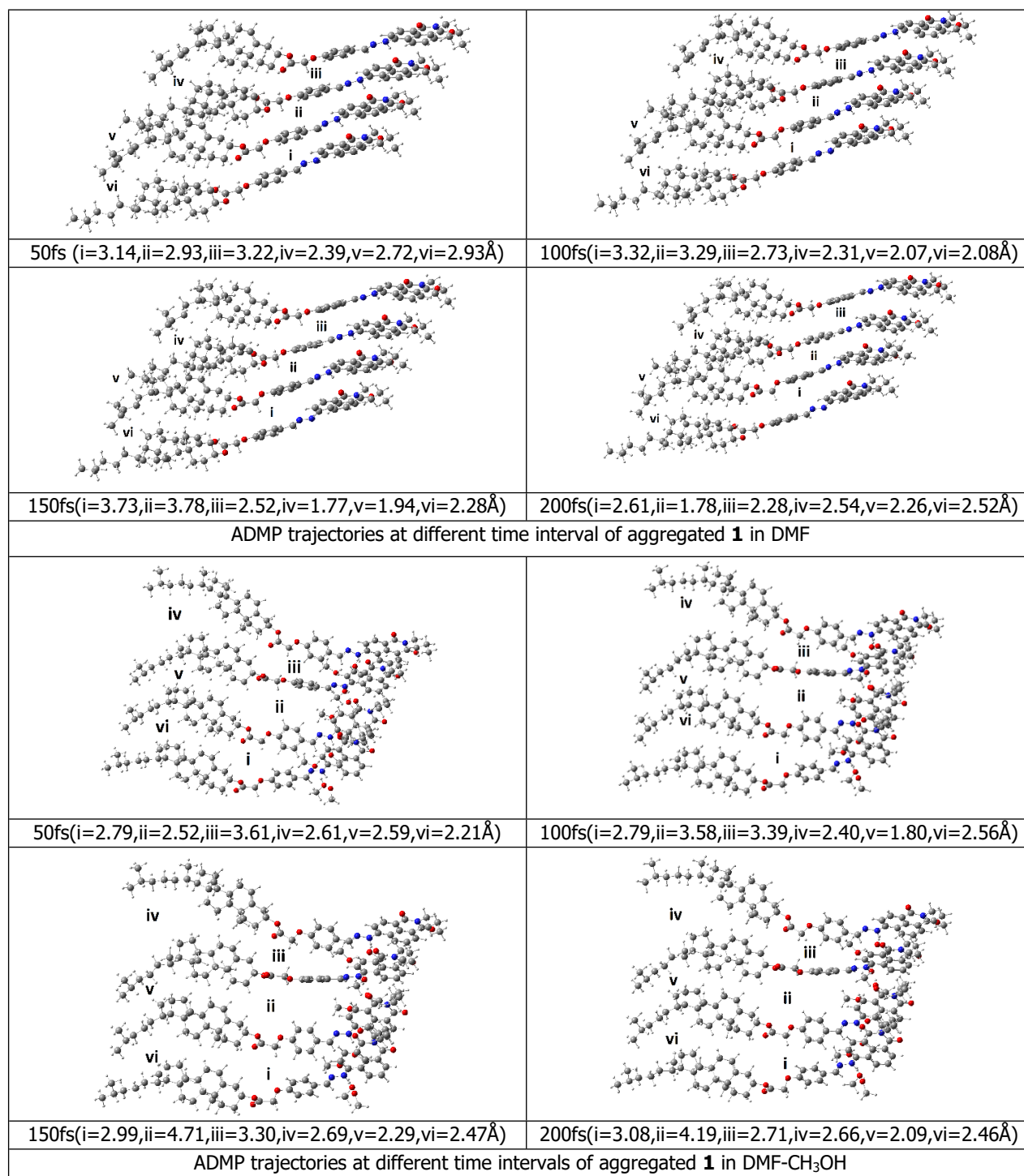
50fs (i=3.14,ii=2.93,iii=3.22,iv=2.39,v=2.72,vi=2.93Å)	100fs(i=3.32,ii=3.29,iii=2.73,iv=2.31,v=2.07,vi=2.08Å)
150fs(i=3.73,ii=3.78,iii=2.52,iv=1.77,v=1.94,vi=2.28Å)	200fs(i=2.61,ii=1.78,iii=2.28,iv=2.54,v=2.26,vi=2.52Å)

ADMP trajectories at different time interval of aggregated **1** in DMF

50fs(i=2.79,ii=2.52,iii=3.61,iv=2.61,v=2.59,vi=2.21Å)	100fs(i=2.79,ii=3.58,iii=3.39,iv=2.40,v=1.80,vi=2.56Å)
150fs(i=2.99,ii=4.71,iii=3.30,iv=2.69,v=2.29,vi=2.47Å)	200fs(i=3.08,ii=4.19,iii=2.71,iv=2.66,v=2.09,vi=2.46Å)

ADMP trajectories at different time intervals of aggregated **1** in DMF-CH$_3$OH

Figure S5. ADMP trajectories in vacuum at different time intervals of aggregated **1**of the optimized geometries in different solvents.
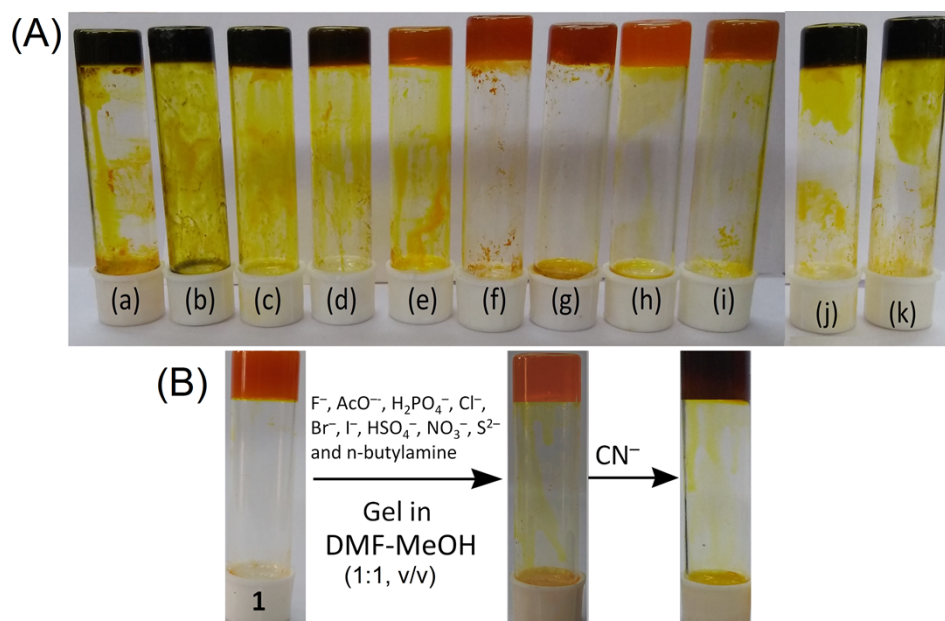
Figure S6. (A) Changes in the gel state of **1** (c= 6.1 x 10^{-2} M) in DMF upon addition of 1 equiv. amount of different anions (as tetrabutylammonium salt) after 15 min [from left to right: (a) CN$^-$, (b) F$^-$, (c) AcO$^-$, (d) H$_2$PO$_4^-$, (e) Cl$^-$, (f) Br$^-$, (g) I$^-$, (h) HSO$_4^-$, (i) NO^{3-}, (j) S^{2-} and (k) n-Butylamine]; (B) Selectivity for CN$^-$ in presence of all other anions (gel concentration was 1.2 x 10^{-2} M).
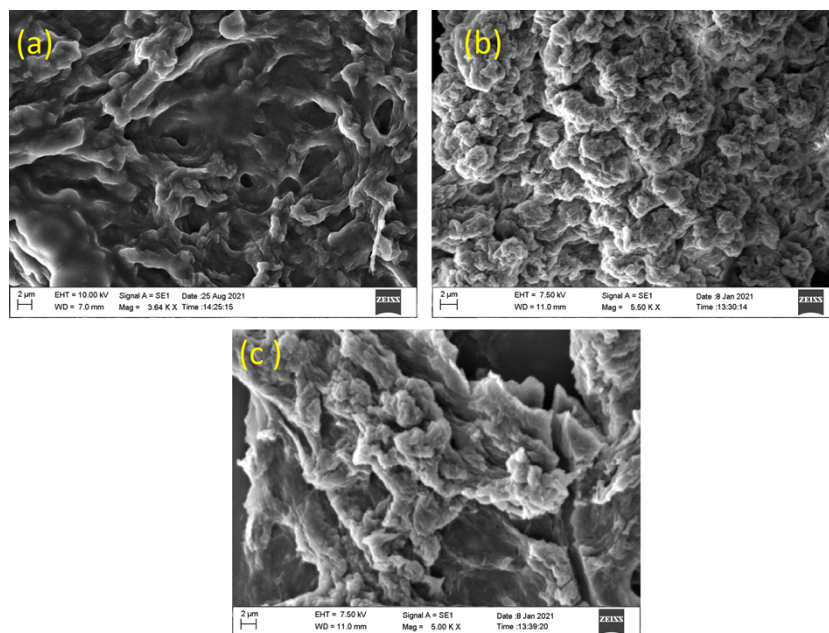

Figure S7. SEM images: (a) F-induced DMF gel (b) CN$^-$-induced DMF gel and CN$^-$- induced DMF- MeOH (1:1, v/v) gel of **1.**
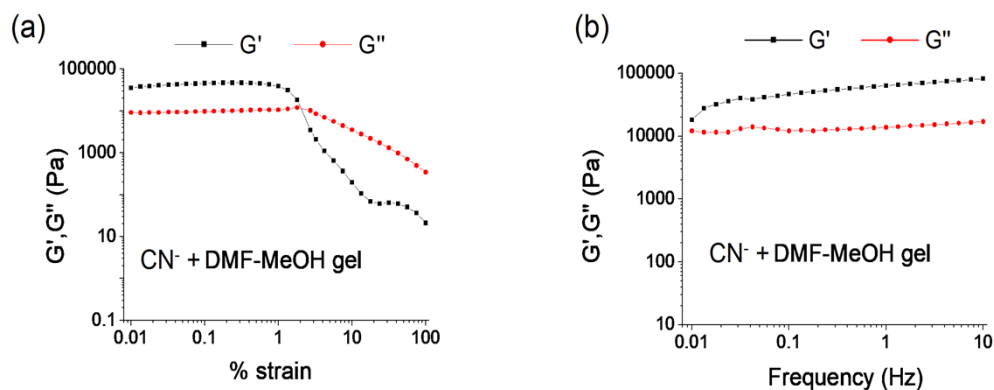
Figure S8. Rheology study of CN⁻-induced gel of **1**; (a) amplitude sweep (at constant frequency of 1 Hz) and (b) frequency sweep (at constant 0.5% strain) experiments [Gel was prepared at mgc (c= 1.2 x 10^{-2} M) and the experiments were carried out at 25 °C].

Table S2. Summary of rheological properties of CN⁻-induced gel of **1**.

Gel in Solvent	Critical strain (%)	Crossover (% strain)	G'_{av} (Pa)*	G''_{av} (Pa)*	G''_{av}/G'_{av}
CN⁻-induced gel in DMF-MeOH	0.74	2.03	63660	14070	0.22

*G'_{av} and G''_{av} values were calculated from frequency sweep data
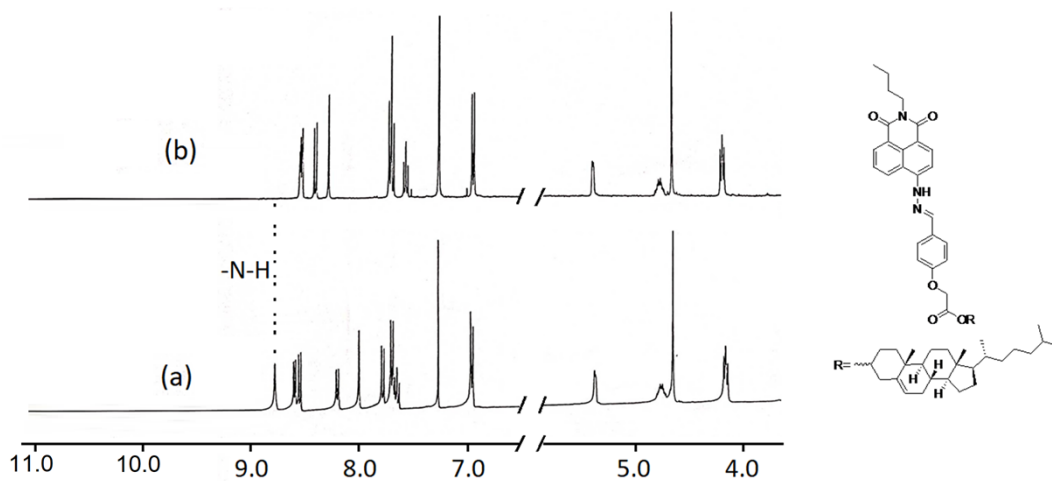
Figure S9. Partial ¹H NMR (400 MHz) of **1** (c= 4.9 x 10^{-3} M) in the absence (a) and presence (b) of an equiv. amount of CN⁻ (c= 0.245 M) in CDCl₃.
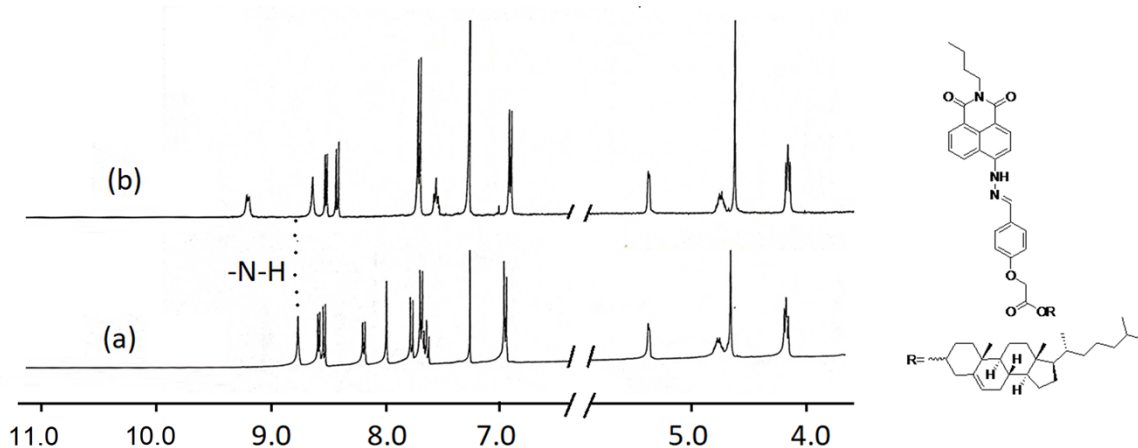
Figure S10. Partial ^{1}H NMR (400 MHz) of **1** (c= 4.9 x 10^{-3} M) in the absence (a) and presence (b) of an equiv. amount of F$^-$ (c= 0.245 M) in CDCl$_3$.
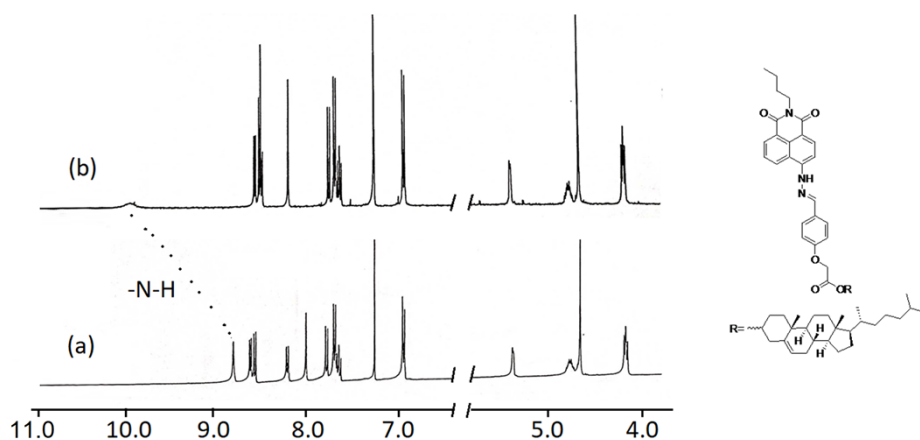

Figure S11. Partial ^{1}H NMR (400 MHz) of **1** (c= 4.9 x 10^{-3} M) in the absence (a) and presence (b) of an equiv. amount of AcO$^-$ (c= 0.245 M) in CDCl$_3$.
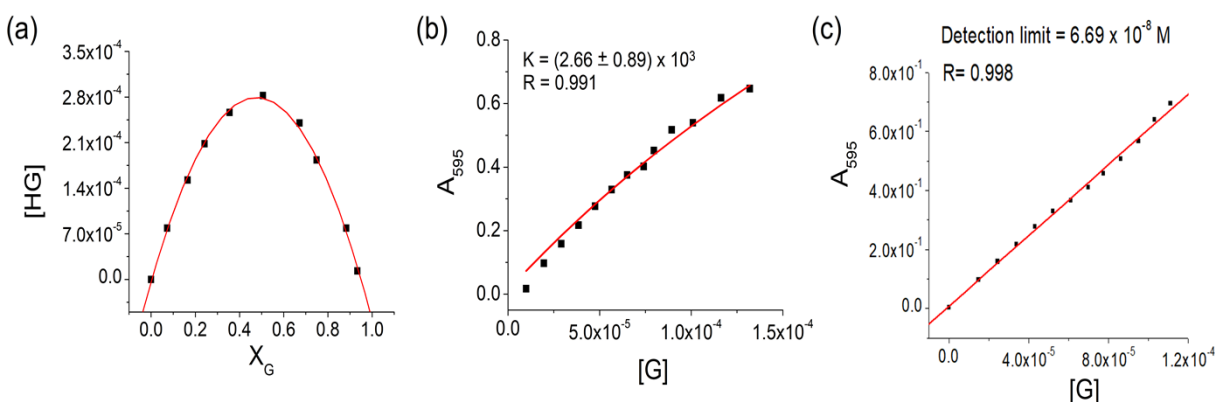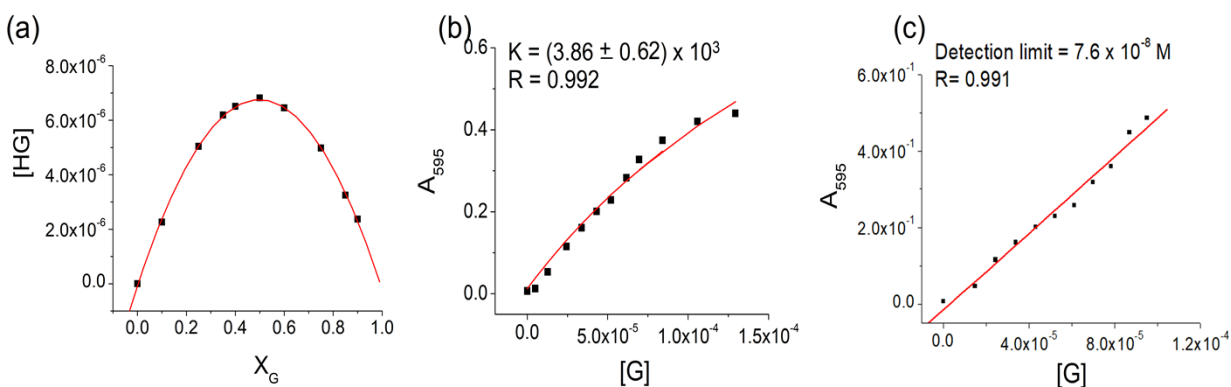

Figure S12. (a) UV-Vis Job's plot of receptor **1** with CN ; (b) Binding constant curve from non-linear fitting UV-Vis titration data and (c) detection limit for CN$^-$ (c = 1.0 x 10^{-3} M) with **1** (c = 2.5.0 x 10^{-5} M) using the data at 595 nm from UV-vis titration in DMF.

Figure S13. (a) UV-Vis Job's plot of receptor **1** with F; (b) Binding constant curve from non-linear fitting UV-Vis titration data and (c) detection limit for F$^-$ (c = 1.0 x 10^{-3} M) with **1** (c= 2.5.0 x 10^{-5} M) using the data at 595 nm from UV-vis titration in DMF.
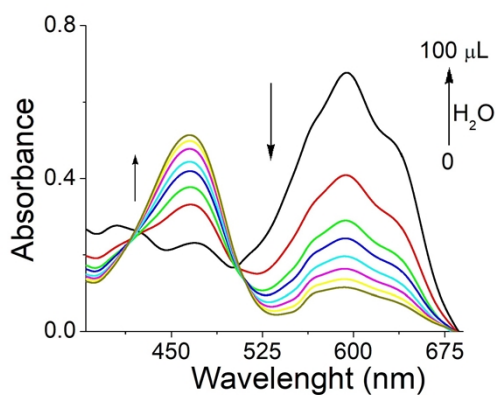

Figure S14. Change in absorbance of **1**.CN$^-$ ensemble [prepared from addition of 6 equiv. of CN$^-$ (c = 1.0 x 10^{-3}) to **1** (c = 2.50 x 10^{-5} M) in DMF] upon addition of H$_2$O.
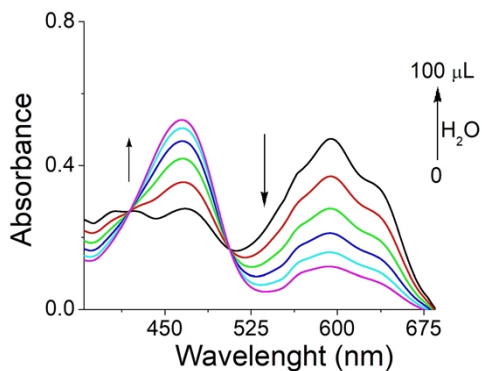

Figure S15. Change in absorbance of **1**.F$^-$ ensemble [prepared from addition of 6 equiv. of F$^-$ (c = 1.0 x 10^{-3}) to **1** (c = 2.50 x 10^{-5} M) in DMF] upon addition of H$_2$O.
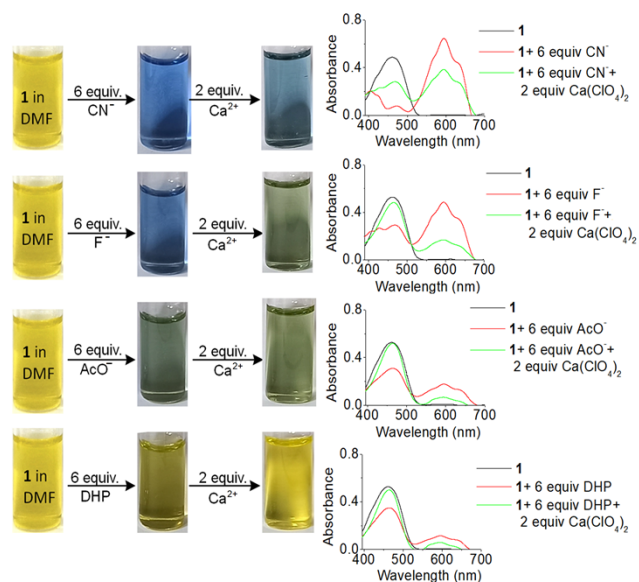
Figure S16. Change in colour of the solution of **1** ($c = 2.50 \times 10^{-5}$ M) in DMF upon addition of 6 equiv. amounts of CN^-, F^-, AcO^- and $H_2PO_4^-$ followed by addition of 2 equiv. amounts of $Ca(ClO_4)_2$.
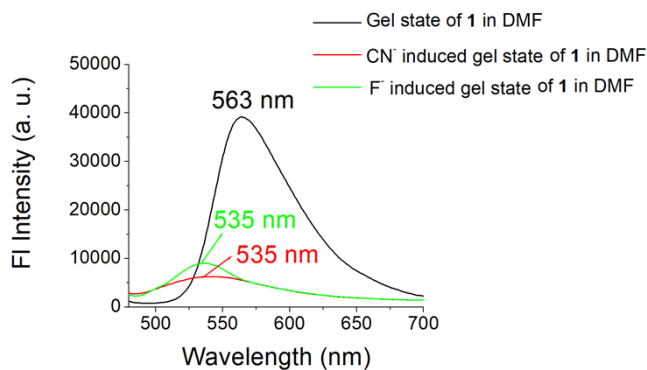

Figure S17. Emission change ($\lambda_{exc} = 460$ nm) in gel state of **1** ($c = 6.1 \times 10^{-2}$ M) in absence and presence of an equiv. amount of anions (CN^- and F^-).
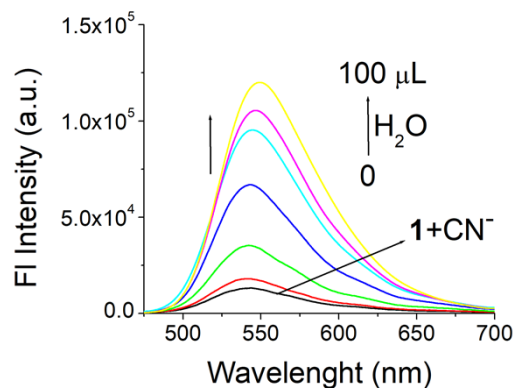

Figure S18. Change in emission of **1**.CN^- ensemble [prepared from addition of 6 equiv. of CN^- ($c = 1.0 \times 10^{-3}$) to **1** ($c = 2.50 \times 10^{-5}$ M) in DMF] upon addition of H_2O ($\lambda_{exc} = 460$ nm).
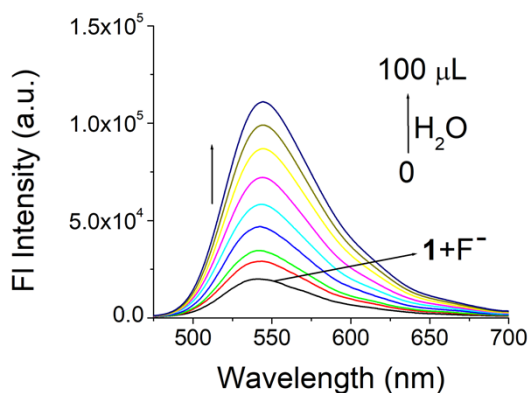
Figure S19. Change in absorbance of **1**.F⁻ ensemble [prepared from addition of 6 equiv. of F⁻ ($c = 1.0 \times 10^{-3}$) to **1** ($c = 2.50 \times 10^{-5}$ M) in DMF] upon addition of H_2O ($\lambda_{exc} = 460$ nm).
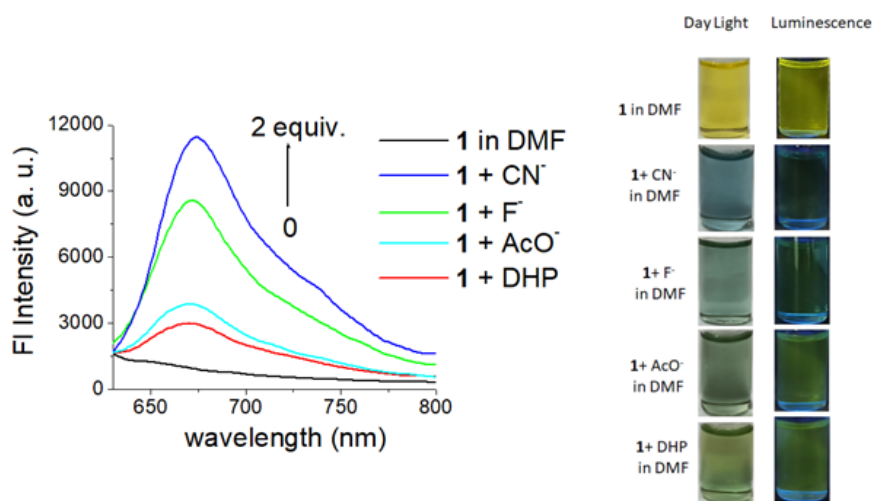

Figure S20. Change in emission of **1** ($c = 2.50 \times 10^{-5}$ M) in DMF upon addition of different anions ($c = 1.0 \times 10^{-3}$ M) ($\lambda_{exc} = 595$ nm).
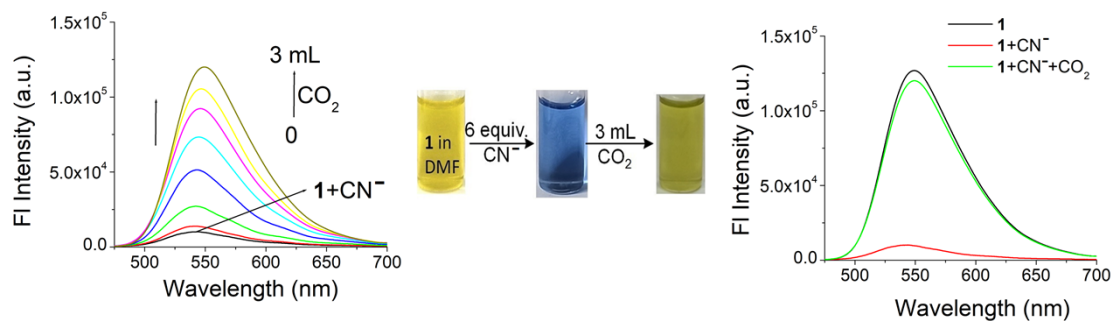

Figure S21. Change in absorbance of **1**.CN⁻ ensemble [prepared from addition of 6 equiv. of CN⁻ ($c = 2.5 \times 10^{-3}$) to **1** ($c = 2.50 \times 10^{-5}$ M) in DMF] upon bubbling of CO_2.
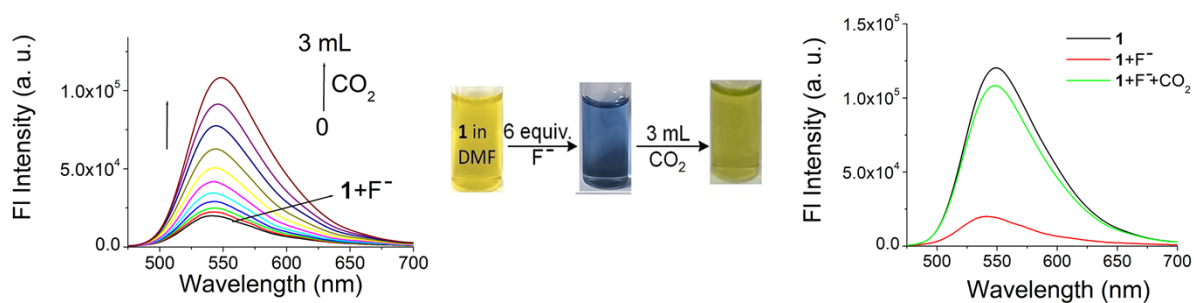
Figure S22. Change in absorbance of **1**.F⁻ ensemble [prepared from addition of 6 equiv. of F⁻ (c = 2.5 x 10⁻³) to **1** (c = 2.50 x 10⁻⁵ M) in DMF] upon bubbling of CO_2.
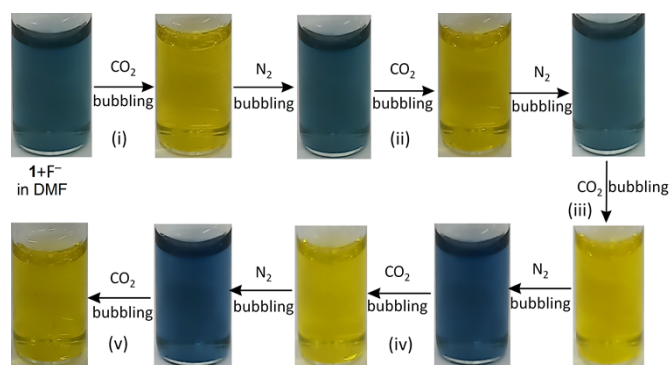

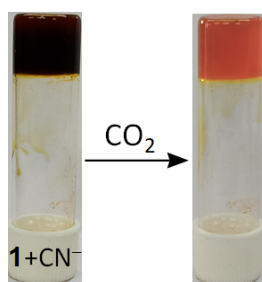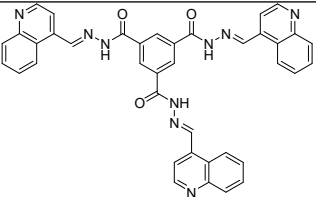**Figure S23.** Pictorial representation of reversibility of gelator **1** in detection of CO_2 gas.
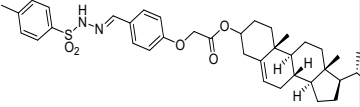
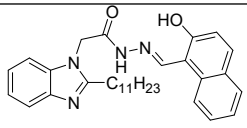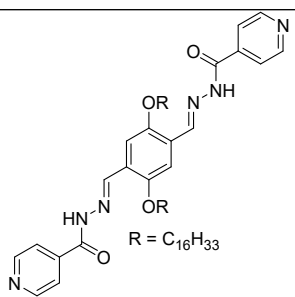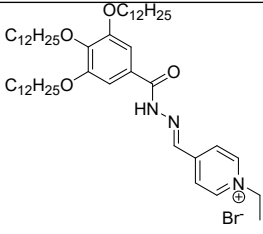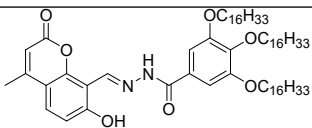**Figure S24.** Detection of CO_2 gas by CN⁻- treated gel (DMF-MeOH; 1:1, v/v) of **1** (c= 1.2 x 10⁻² M).
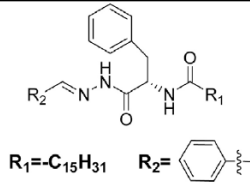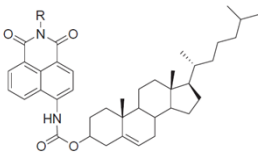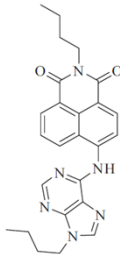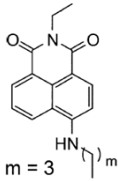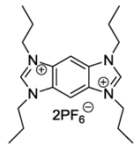
Table S3. Reported structures for cyanide sensing in gel phase through deprotonation mechanism.

Sl. No.	Structure	Medium	Mode of interaction/ phase change	Interference	Detection limits in solution study	Ref. no.
1.		DMSO/H_2O (1:1 v/v)	Deprotonation, gel-to-sol transition	-	1.5×10^{-6} M	1
2.		DMSO/H_2O (1:1 v/v)	Deprotonation, gel-to-sol transition	F^-	7.96×10^{-5} M	2
3.		glycerol	Deprotonation, gel-to-gel transition	Al^{3+} and Fe^{3+}	3.02×10^{-6} M	3
4.		THF	Deprotonation, gel-to-sol transition	-	1.12×10^{-5} M	4
5.		DMSO/H_2O (1:1 v/v)	Deprotonation, gel-to-sol transition	-	3.68×10^{-7} M	5
6.		n-BuOH/H_2O (9:1 v/v)	Deprotonation, gel-to-sol transition	S^{2-}	1.64×10^{-8} M	6

	Structure	Medium	Mechanism	Anions		Ref. No.
7.		DMSO	Deprotonation, gel-to-sol transition	F⁻, AcO⁻	-	7
8.		DMSO-H_2O	H-bonding followed by deprotonation, gel-to-gel transition	F⁻, AcO⁻, $H_2PO_4^-$	-	8
9.		DMF/H_2O (1/1, v/v)	Deprotonation	-	5.53×10^{-7} M	9
10.		DMF/MeOH (1/1, v/v)	Deprotonation gel-to-gel transition	-	6.69×10^{-8} M	Our work

Table S4. Reported structures for CO_2 sensing in gel-sol medium.

Sl. No.	Structure	Medium	Solvent	Ref. No.
13.		solution	CH_3CN	10
14.		gel and solution	DMSO	11

15.	 R_1=-$C_{15}H_{31}$ R_2=	gel and solution	DMSO	12
16.	 R = -(CH$_2$)$_2$O(CH$_2$)$_2$OH R = -(CH$_2$)$_2$O(CH$_2$)$_2$O(C=O)CH$_3$	gel and solution	DMSO	13.
17.		solution	CH$_3$CN containing 1% DMSO	14.
18.	 m = 3	solution	DMSO	15.
19.	 2PF$_6$	solution	CH$_3$CN	16.

^{1}H NMR (CDCl$_3$, 400MHz)

COSY of 1 (CDCl$_3$, 400 MHz)

^{13}C NMR (CDCl$_3$, 100MHz)

13.8

11.8

Mass spectrum of 1

AD_SD_R3rep.d: +MS, 0.1-0.1min #3-8

274.2696

814.5181

calcd. C$_{52}$H$_{68}$N$_3$O$_5$ [M+H+] 814.5159, found 814.5181 [M+H+].

409.1549

1650.9803
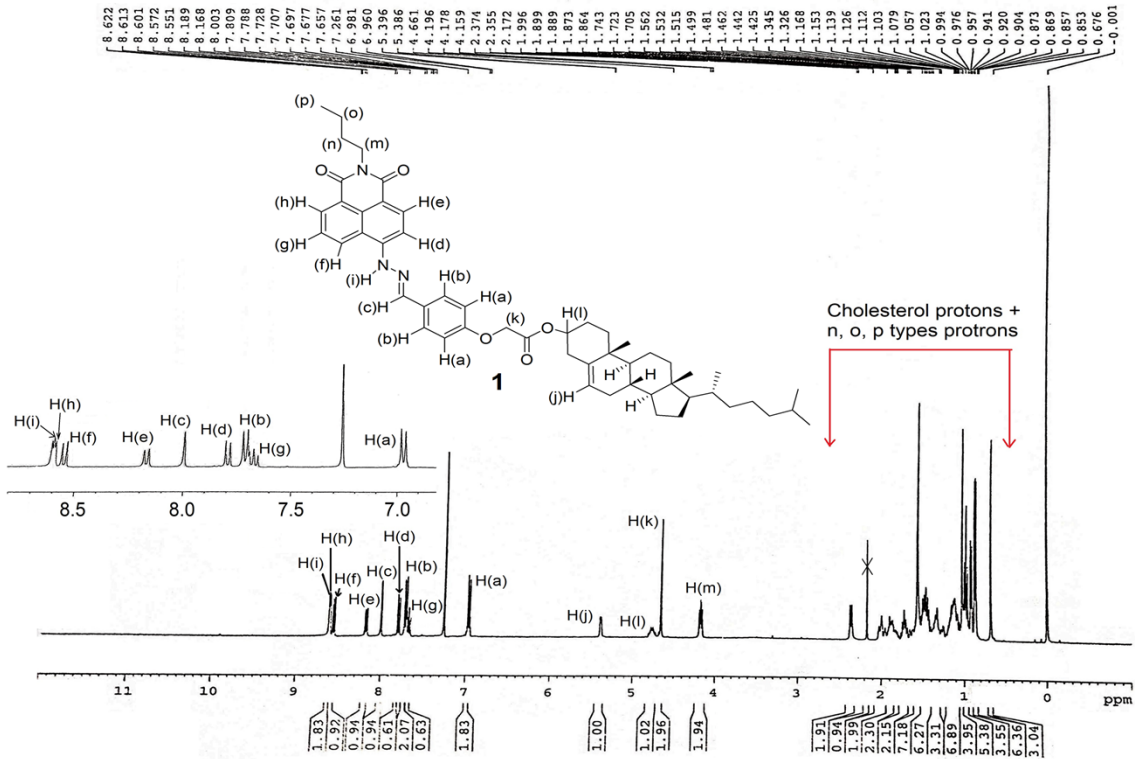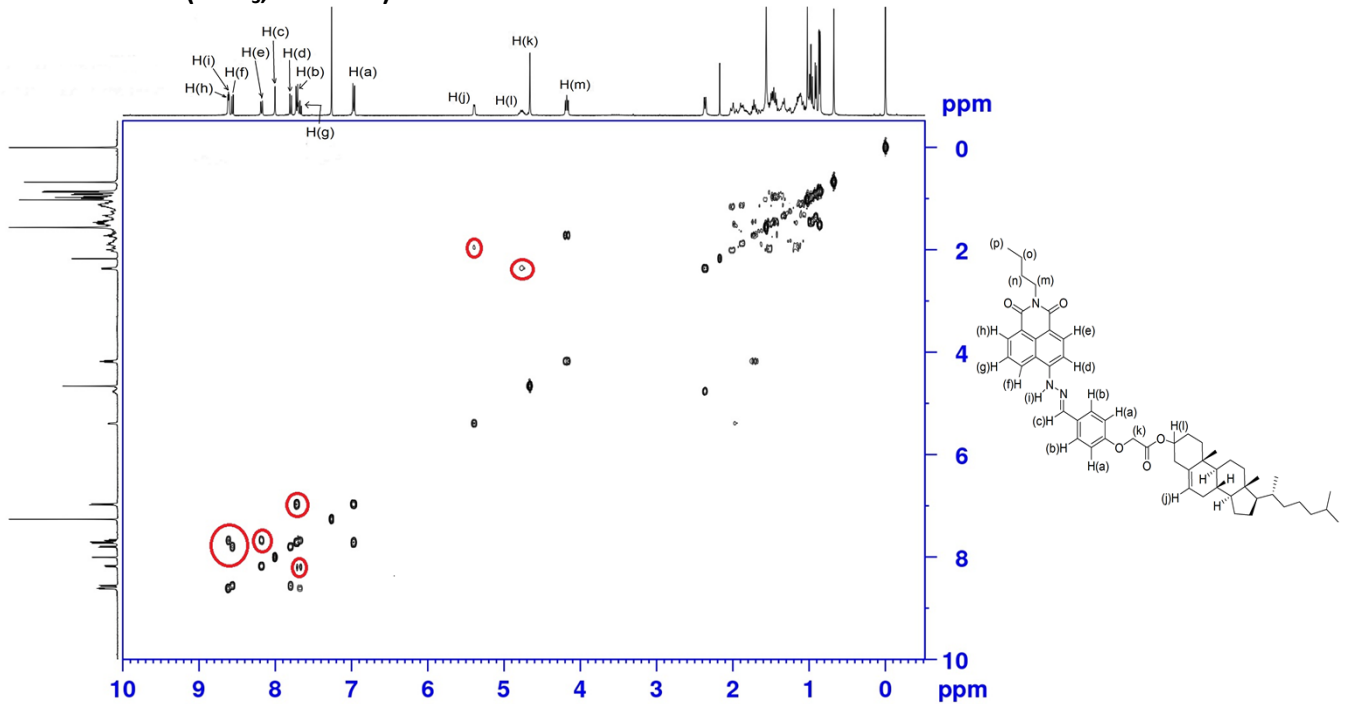
References:

1. S. Sharma, M. Kumari, N. Singh, *Soft Matter.*, 2020, **16**, 6532–6538.

2. A. Panja, S. Ghosh and K. Ghosh, *New J. Chem*., 201**9**, **43**, 10270–10277.

3. H. Yao, J. Wang, S.-S. Song, Y.-Q. Fan, X.-W. Guan, Q. Zhou, T.-B. Wei, Q. Lin and Y.-M. Zhang, *New J. Chem*., 2018, **42**, 18059–18065.

4. S. K. Samanta, N. Dey, N. Kumari, D. Biswakarma and S. Bhattacharya, *ACS Sustainable Chem. Eng*., 2019, **7**, 12304–12314.

5. B. Sarkar, P. Prabakaran, E. Prasad and R. L. Gardas, ACS Sustainable Chem. Eng., 2020, **8**, 8327–8337.

6. J.-H. Hu, Z.-Y. Yin, K. Gui, Q.-Q. Fu, Y. Yao, X.-M. Fu and H.-X. Liu, *Soft Matter*, 2020, **16**, 1029–1033.

7. K. Ghosh and C. Pati, *Tetrahedron Lett.*, 2016, **57**, 5469-5474.

8. S.-N. Li, B. Li, L.-X. Gong, Z.-R. Yu, Y. Feng, D. Jia, Y. Zhou, L.-C. Tang, *Mater. Des*., 2019,**162**, 162–170.

9. S. Ghosh, P. Jana and K. Ghosh, *Anal. Methods*, 2021, **13**, 695–702.

10. M. Lee, S. Jo, D. Lee, Z. Xu and J. Yoon, *Dyes Pigm*., 2015, **120**, 288-192.

11. X. Zhang, Y. Song, M. Liu, H. Li, H. Sun, M. Sun and H. Yu, *Dyes Pigm*., 2019, **160**, 799-805.

12. X. Zhang, H. Mu, H. Li, Y. Zhang, M. An, X. Zhang, J. Yoon and H. Yu, *Sensors and Actuators B: Chemical*, 2018, **255**, 2764-2778.

13. X. Zhang, H. Li, H. Mu, Y. Liu, Y. Guan, J. Yoon and H. Yu, *Dyes Pigm*., 2017, **147**, 40-49.

14. C. Pati, R. Raza and K. Ghosh, *Spectrochim. Acta A*, 2020, **229**, 117910.

15. T. Gunnlaugsson, P. E. Kruger, P. Jensen, F. M Pfeffer and G.M.Hussey, *Tetrahedron Lett*., 2003**, 44**, 8909e13.

16. Z. Guo, N.R. Song, J.H. Moon, M. Kim, E.J. Jun, J. Choi, J. Y. Lee, C. W. Bielawski, J. L. Sessler, and J. Yoon, *J Am Chem Soc*., 2012, **134**, 17846e9.